Published in final edited form as:
Hum Mol Genet. 2005 January 1; 14(1): 49–57.

Deficiency of pantothenate kinase 2 (*Pank2*) in mice leads to retinal degeneration and azoospermia

Yien-Ming Kuo[1,2,5], **Jacque L. Duncan**[3], **Shawn K. Westaway**[6], **Haidong Yang**[3], **George Nune**[3], **Eugene Yujun Xu**[4], **Susan J. Hayflick**[6], and **Jane Gitschier**[1,2,5,*]

1*Department of Medicine, University of California, San Francisco, CA, USA*

2*Department of Pediatrics, University of California, San Francisco, CA, USA*

3*Department of Ophthalmology, University of California, San Francisco, CA, USA*

4*Department of Obstetrics, Gynecology and Reproductive Sciences, University of California, San Francisco, CA, USA*

5*Howard Hughes Medical Institute, University of California, San Francisco, CA, USA*

6*Department of Molecular and Medical Genetics, Oregon Health and Science University, OR, USA*

Abstract

Pantothenate kinase-associated neurodegeneration (PKAN, formerly known as Hallervorden–Spatz syndrome) is a rare but devastating neurodegenerative disorder, resulting from an inherited defect in coenzyme A biosynthesis. As pathology in the human condition is limited to the central nervous system, specifically the retina and globus pallidus, we have generated a mouse knock-out of the orthologous murine gene (*Pank2*) to enhance our understanding of the mechanisms of disease and to serve as a testing ground for therapies. Over time, the homozygous null mice manifest retinal degeneration, as evidenced by electroretinography, light microscopy and pupillometry response. Specifically, *Pank2* mice show progressive photoreceptor decline, with significantly lower scotopic a- and b-wave amplitudes, decreased cell number and disruption of the outer segment and reduced pupillary constriction response when compared with those of wild-type littermates. Additionally, the homozygous male mutants are infertile due to azoospermia, a condition that was not appreciated in the human. Arrest occurs in spermiogenesis, with complete absence of elongated and mature spermatids. In contrast to the human, however, no changes were observed in the basal ganglia by MRI or by histological exam, nor were there signs of dystonia, even after following the mice for one year. *Pank2* mice are 20% decreased in weight when compared with their wild-type littermates; however, dysphagia was not apparent. Immunohistochemistry shows staining consistent with localization of Pank2 to the mitochondria in both the retina and the spermatozoa.

INTRODUCTION

Coenzyme A (CoA) is a ubiquitous metabolic substrate, an essential ingredient in the tricarboxylic acid cycle, in the fatty acid metabolism and in the synthesis of some amino acids. CoA is synthesized from vitamin B5 (pantothenic acid) in a series of five enzymatic steps, the first of which is catalyzed by pantothenate kinase.

Four human isoforms of pantothenate kinase are now known, and defects in one of these, pantothenate kinase 2 (PANK2), causes a fatal, inherited neurodegenerative disease formerly known as Hallervorden–Spatz syndrome (HSS), but now referred to as pantothenate kinase-

*To whom correspondence should be addressed at: HSE-901, PO Box 0794, University of California, San Francisco, CA 94143, USA. Tel: +1 4154768729; Fax: +1 4155020720; Email: gitschi@itsa.ucsf.edu.

associated neurodegeneration (PKAN) (1). This disorder typically presents in early childhood with disturbances in gait, dystonia, dysarthria and dysphagia (2). A primary site of degeneration is the globus pallidus, in which cellular tissue is replaced by iron, culminating in a characteristic image called 'eye of the tiger' on T2-weighted magnetic resonance. Typically, the retina is also affected, leading to retinitis pigmentosa.

How might a defect in PANK2 give rise to such specific and consistent neuropathology? Some insight into this question was gained by the discovery that, of the four pantothenate kinases in mammals, PANK2 is probably uniquely targeted to the mitochondria (3,4), strongly suggesting a role for this paralog in energy metabolism. Possibly, tissues which require high energy utilization and which are exquisitely sensitive to oxygen deprivation, such as the globus pallidus, are particularly vulnerable to perturbations in pantothenatemetabolism. Disruptions in fatty acid and amino acid metabolisms are other likely consequences of PANK2 deficiency. A secondary question of how a defect in PANK2 results in iron dysregulation in the central nervous system also remains unanswered.

To assist in addressing these questions, we turned to the experimentally tractable mouse model. Here, we describe the generation and analysis of a homozygous mutant animal, *Pank2*, deficient in pantothenate kinase 2, the murine ortholog of human PANK2 (1).

RESULTS

Generation of *Pank2* mice

Using standard targeting techniques, we generated a null mutation in *Pank2* by replacing the 3′ half of exon 2 and part of the adjacent intron with an *nlac/neo*^{R} cassette (Fig. 1A). As the enzymatic activity of Pank2 is likely encoded by exons 2–7 (1), this strategy promised to result in a complete disruption of pantothenate kinase function.

Following the development of knock-out ES cell lines, we generated animals from two of these (81 and 174), with indistinguishable phenotypic results. For both lines, homozygous mutant mice, ascertained by PCR genotyping (Fig. 1B), were viable and were produced in the expected Mendelian ratio of 1:2:1.

Two types of analyses confirmed that the *Pank2* gene was inactivated in the resulting mice. First, by RT–PCR across exons 2–4, no transcript corresponding to *Pank2* was detected in a variety of tissues derived from the knock-out animals (Fig. 1C). RT–PCR across translation-initiating exon 1C and the β-galactosidase gene detected transcript in various *Pank2* (−/−) tissues, but not in wild-type (+/+) organs (data not shown), further confirming the correct targeting. Second, western analysis with an antibody directed against a sequence encoded uniquely by the first *Pank2* exon, verified the absence of the expected 50 kDa Pank2 protein in testes from the mutant mice (Fig. 1D).

Growth and viability

Because human patients with PKAN develop difficulty in eating and swallowing (dysphagia), we monitored the mice for feeding difficulties and for growth. A reduction in the size of *Pank2* knock-out mice of both sexes was readily apparent, with weekly body-weight measurements indicating differences from 3 weeks of age until ~56 weeks of age (Fig. 2). Weight in the mutant animals was roughly 80% that of their wild-type and heterozygous counterparts (heterozygotes not shown). Although body length was not routinely measured, the mutant mice were also obviously shorter (Fig. 2, inset).

However, by video monitoring, we saw no difficulties with either food access or eating behavior. In addition, we found no reduction in the daily food intake (roughly assessed by

weighing food) between wild-type and mutant animals, which were housed separately. Thus, we conclude that retardation in growth is not due to dysphagia in the mice or to an inability of mice to compete for food, but more likely due to a metabolic difference in these mice brought on by inactivation of Pank2.

Fertility

Fertility problems became apparent upon attempting to breed homozygous *Pank2* animals. Female knock-out mice, mated with wild-type males, produced viable offspring but much fewer in number when compared with wild-type or heterozygote females, probably reflecting an *in utero* effect of maternal Pank2 deficiency. In contrast, the reciprocal cross of *Pank2* males with wild-type females resulted in no viable offspring or no visible pregnancies, despite the presence of coital plugs. These findings suggested male infertility in the mutant animals.

Measurements of testis weight and epididymal sperm content confirmed a defect in spermatogenesis of *Pank2* males. Although testis weight was comparable in the sexually immature mice at 2 weeks of age, at 6 weeks, an age at which mice typically reach reproductive maturity, *Pank2* males had smaller testes (Fig. 3A) and lacked sperm in the epididymis. The weight discrepancy, greater than that could be accounted for by overall body-weight difference, as well as the azoospermia continued when followed through 1 year of life. Azoospermia was not a result of hormone insufficiency; testosterone, luteinizing hormone and follicle-stimulating hormone were comparable to wild-type (data not shown).

Histological analyses revealed a complete absence of elongated spermatids in the seminiferous tubules of *Pank2* mice. For example, as shown in Figure 3B, at 40× magnification, mature elongated spermatozoa are seen in the lumen of wild-type animals, but are completely absent in the *Pank2* mutant. At 100×, only round spermatids are present near the lumenal border of the mutant tubule. These fail to elongate, and instead, appear to accumulate vacuoles. When compared with normal spermatogenesis, in which maturation into haploid spermatids occurs in a synchronous and spatially orderly process, the spermatocytes and spermatids are somewhat disordered in the *Pank2* testes tubule. This finding could besecondary to the arrest at the round spermatid stage, as has been reported in other mutants (5).

Neurological assessment

The *Pank2* animals were continually monitored for evidence of basal ganglia degeneration and iron accumulation, as these are hallmarks of the human disease. Mutant animals up to and including 1 year of age showed no evidence for iron accumulation by MRI or by Perls-DAB staining (see Materials and Methods; data not shown). Tests for neurological impairment, including gait and grip (6), showed no differences between wild-type and *Pank2* homozygous mice tested weekly until 16 months of age.

Retinal examination

Pank2 mutant animals were found to have progressive retinal impairment by three measures: electrorectinography (ERG), pupillary response and histochemistry.

First, the ERG data reflect progressive decline in photoreceptor function in *Pank2* mice when compared with their wild-type littermates. Figure 4A shows a series of representative scotopic (dark-adapted) and photopic (light-adapted) waveforms recorded from wild-type and mutant mice at two ages (P84 and P411), and Figure 4B summarizes the ERG amplitude data for all animals tested at P84, P285 and P362–P430 (data for the later ages collapsed into a single time point for average age of P385). One-way analysis of variance (ANOVA) was significant ($P < 0.0001$ for scotopic a- and b-waves, and $P < 0.002$ for photopic b-waves) with the decline with age in the mutant accounting for the difference (Bonferroni post-test analysis, P84 versus P385

$P < 0.05$ for a-waves and $P < 0.01$ for scotopic and photopic b-waves). In contrast, no significant differences were noted in amplitudes with age for the wild-type ($P > 0.05$ for all three). Although the scotopic a- and b-wave responses were similar at P84, at 1 year, the amplitudes were reduced by 25 and 16%, respectively, when compared with those of wild-type. ERGs from heterozygote animals were comparable to wild-type (data not shown).

Second, the pupillary light response, which can serve as an additional indication of photoreceptor degeneration/dysfunction (7), was also diminished in the mutant. A summary of pupil responses of the *Pank2* mice compared with those of the wild-type littermates at P365 is presented in Figure 4C. Constriction in the mutant animals was both slower and less complete in response to light than that in the wild-type littermates. This result is consistent with the progressive photoreceptor dysfunction demonstrated in ERG recordings among older *Pank2* mice.

Third, histological analysis revealed gross abnormalities in the retinal layers corresponding to the rods and cones in *Pank2* animals over 1 year of age, consistent with the ERG and pupillary findings. As shown by the sections in Figure 4D, taken at P411, the rod outer segment (OS) and inner segment (IS) in the mutant animal are thinner than those of the wild-type, and the OS is laden with vacuoles. The outer nuclear layer (ONL) layer, which houses the cellbodies for the rods and cones, has fewer cells than in the age-matched wild-type. The remaining layers, the outer plexiform layer (OPL), inner nuclear layer INL, inner plexiform layer (IPL) and ganglion cell layer (GCL) are indistinguishable from wild-type. Figure 4E summarizes the retinal thickness data for animals P363 and older. At P84, no differences in retinal structure between *Pank2* and wild-type mice were apparent (data not shown).

Immunolocalization of Pank2 in testes and retina

Immunohistochemical analysis of normal mouse testis and retina with an anti-Pank2 antibody revealed a pattern consistent with localization of Pank2 to the mitochondria, as predicted by previous studies (3,4).

As shown in Figure 5A, staining in the tubule of a wild-type testis reveals discrete intense localization to the elongated spermatids, most likely corresponding to densely fused mitochondria in the mitochondrial mid-piece of the mature spermatozoan.

In the retina (Fig. 5B), Pank2 is found in many layers, including the outer plexiform layer (OPL), inner nuclear layer (INL) and inner plexiform layer (IPL), but the most intense staining is observed within the photoreceptor itself, at the inner segment (IS), the seat of mitochondria and Golgi apparatus. Immunofluorescence with anti-Pank2 antibody and with an antibody against a mitochondria-specific antibody (anti-OxPhos Complex V) showed co-localization, further supporting targeting of Pank2 to this organelle (data not shown). In contrast, another member of the pantothenate kinase family, Pank1A, is dispersed throughout the photoreceptor, including the outer and inner segments and the outer nuclear layer (Fig. 5C), thus controlling for the specificity of Pank2 localization.

Thus, for these two tissues, it is noteworthy that the cell types harboring the most intense staining of Pank2 are precisely those that are most affected in the mutant animals.

DISCUSSION

We describe a mouse lacking pantothenate kinase 2, the enzyme deficient in the severe, neurodegenerative human disease PKAN (formerly HSS). We demonstrate that a defect in Pank2 causes growth retardation, azoospermia and retinal degeneration. As Pank2 is targeted

to the mitochondria, these phenotypes likely reflect a defect in utilization of vitamin B5 in this organelle.

The most striking finding in the mutant animals was azoospermia. Infertility in human males with PKAN has not been previously described, or to our knowledge even considered, as most individuals with PKAN are so severely impaired that they die before adulthood. Conversely, patients with atypical disease, characterized by late-onset development of symptoms, are not found to have null mutations of the *PANK2* gene (8). Although we are unaware of any adult male patients with offspring, we have confirmed that at least one adult male, who is a compound heterozygote for two missense mutations in the *PANK2* gene, produces viable sperm.

In contrast, male sterility had been noted in the *fumble* fly, a *Drosophila* hypomorphic mutant of pantothenate kinase (9). Indeed, the *fumble* mutant was identified initially in a screen for male sterility by P-element mutagenesis (10) and was later found to be defective in spermatogenesis. In drawing comparisons between these two model animals, however, two differences between the fly and mammalian pantothenate kinases should be appreciated. First, in the human and mouse, different isoforms of pantothenate kinase, likely targeted to different subcellular compartments, are encoded by four different genes (1), whereas in *Drosophilia*, a single pantothenate kinase core gene encodes three different isoforms, differing only by their N-terminal, and is thus responsible for all pantothenate kinase activity within the cell. Second, although a null mutation in the murine *Pank2* gene is the subject of the present study, the *Drosophila* mutant is hypomorphic. Thus, unlike the murine model, in which the pantothenate kinase defect is likely to be mitochondria-specific, the fumble fly is presumably partially deficient in pantothenate kinase activity in all subcellular compartments.

The sterility defect in the *Pank2* mouse appears to lie in the inability of the round spermatid to elongate and mature into the spermatozoan. This arrest in spermiogenesis (at approximately step 5) is a feature in several other murine knock-out mutants, including the *CREM*-deficient mutant (11,12) and the *miwi* mutant (15). CREM has been shown to be a master regulator of genes involved in spermiogenesis, and MIWI appears to effect reduced expression of CREM target genes by direct mRNA interaction. Whether or how Pank2 plays into this master regulation of spermiogenesis remains to be examined.

A simpler explanation for the arrest could lie in the inability of the mutant cells to support the metabolic needs for spermiogenesis, which involves extensive remodeling. Metabolic demand is also a feature of the photoreceptor in the renewal of the rod outer segment. As the concentration of Pank2 by immunohistochemistry is highest in the two cell types for which abnormalities are found, namely spermatids and photoreceptors, it is tempting to ascribe a cell-autologous defect in Pank2 deficiency.

However, it is worth considering that the photoreceptor and spermatid share another common feature, namely use of support cells in the form of the retinal pigment epithelium (RPE) and Sertoli cells, which are responsible for the metabolism of shed disks from the photoreceptor and extruded cytoplasm from maturing sperm, respectively. This hypothesis has precedent in the *ClC*-2 mouse mutant, in which degeneration of male germ cells and photoreceptors is secondary to a defect in the Sertoli cells and the RPE (13), and in the *Mer* knock-out mouse (14), in which a phagocytic defect in the RPE leads to retinal dystrophy, and which, when combined with knock-outs in related proteins Tyro 3 and Axl, results in azoospermia secondary to a Sertoli cell defect (15). Although the RPE and Sertoli cells appear normal by light microscopy and histochemistry in the *Pank2* mutant, this hypothesis can be assessed by cell-specific transgenic expression and/or cell transplantation studies (16).

An additional argument for this hypothesis is our finding of vacuoles in the OS of the *Pank2* mutant retina. Of the numerous inherited retinal degenerations described in rodents, such

vacuoles are an uncommon feature. Notably, they have been reported in the murine mutants *Mer* (and its counterpart, the *RCS* rat) and *IRBP* (17), whose primary defects lie in the RPE and in the interphotoreceptor matrix, respectively. Thus, a deficiency in Pank2 not only provides an opportunity to study retinal degeneration resulting from perturbations in CoA metabolism, but also sheds further light on the interplay between photoreceptor OS and the RPE.

Although the retinal degeneration in the *Pank2* mice provides a model for studying retinitis pigmentosa in PKAN patients, the mutant failed to exhibit the movement disorder and pathology of the globus pallidus characteristic of the disease, even when followed over 16 months of age and when backcrossed seven generations into a C57/BL6J background. Recently, we embarked on several strategies to provoke a neurological phenotype in the mutant animals by taking advantage of predicted vulnerabilities in the mutant. Our preliminary investigation suggests that deprivation of vitamin-B5 in the diet can elicit gait problems in the mutant animal compared to the wild-type; however, significant morbidity in animals of both genotypes was observed. A more extensive and refined analysis of the long-term consequences of B5 deficiency in the mutant and wild-type is on-going.

MATERIALS AND METHODS

Isolation of the murine *Pank2* gene

We obtained and sequenced a murine expressed sequence tag orthologous to human *PANK2* from Research Genetics. The 3′ UTR unique to *Pank2* was used as a probe for isolation of full-length genomic clones from a 129/SvJ mouse genomic library (Stratagene). Several genomic clones that span exons 2–5 of the mouse *Pank2* gene were recovered, mapped and sequenced.

Targeted deletion of *Pank2*

A targeting vector was constructed to mediate replacement of a 2332 nt *Bam* H1-*Kpn*1 fragment, encoding half of exon 2 and part of intron 2, with a cassette containing nuclear *lacZ* (*nlacZ*) and a neomycin-resistance gene (*neo* R) driven by the *pol* II promoter (18), as shown in Figure 1A. Following sequence confirmation, the targeting construct was linearized and electroporated into JM1 129/SvJ embryonic stem (ES) cells. Correctly targeted ES cell colonies were identified by PCR using two pairs of primers (Fig. 1A). For further confirmation, DNAs from targeted ES cells were analyzed by Southern blot.

Two correctly targeted ES cell lines, 81 and 174, were used to produce chimeras. The F1 heterozygotes were generated by breeding the chimeras with C57BL/6 female mice (Jackson Laboratories), and germline transmission was established.

Confirmation of null animals by genotyping: RT–PCR and western analysis

Genotypes were assessed routinely by PCR amplification of genomic DNA prepared from mouse tails using pairs of *Pank2* primers and a primer specific for neomycin®, yielding 446 and 344 bp products for the wild-type and mutant alleles, respectively (Fig. 1B).

RNA was isolated from mouse brain and testis stored in RNAlater solution using the Totally RNA kit (Ambion). *Pank2* mRNA was amplified by sequential RT–PCR from 1 μg total RNA with the Omniscript kit and PCR kit according to manufacturer's instructions (Qiagen).

For western analysis, a polyclonal rabbit anti-mouse Pank2 antibody was raised against a 14-mer peptide (SGEAESVRRERPGS) in exon 1C (1) and was affinity purified with the peptide. Protein from mouse brain and testes was isolated, resolved on SDS–PAGE gels, and probed with anti-Pank2 antibodies (19).

Testis dissection and fertility testing

Testes were dissected free from fat tissue and epididymis, and were weighed. Sperm content was examined from a single epididymis as described by Lu and Bishop (20). For fertility testing, a *Pank2* mutant male was caged with two mature wild-type females. Conversely, *Pank2* mutant females were caged with a mature wild-type male. Copulation was checked by the presence of the coital plug.

Histological analyses

Testes were fixed in Bouins solution (Sigma) overnight at room temperature, dehydrated, embedded in paraffin and cut (5 μm thickness) as previously described (21). Sections were either stained with Gill's H&E (Vector Laboratories) or immunostained (discussed subsequently).

Eyes were prepared as previously described (14). Sections (1 μm thickness) of the entire retina were cut and stained with toluidine blue as previously described (22,23). Tissue sections were chosen where the rod OS and Müller cell processes crossing the inner plexiform layer were continuous in the plane of section, or nearly so, to ensure that the sections were not oblique (14). The ONL, OS and IS lengths were measured using bioquantification software with a digitizing tablet and camera lucida.

Behavioral tests

A series of behavioral tests were performed as described by Crawley (12). Briefly, for preliminary assessment of general motor activity, animals were tested in an open field (5 min test sessions) and video-taped to evaluate any gross abnormalities in locomotion. The tail suspension test was performed by suspending the mouse by the tail and observing for passivity, trunk curl, limb grasping, visual placing and grip strength. The vertical pole test was used for measuring motor coordination and balance. Mice walking on level and inclined metal screens were observed for missteps, defined as placing any paw between the grids. The hanging wire test was used to evaluate muscle strength of front- and hind-paws. A mouse requires balance and grip strength to suspend its body from the wire. The length of time that the mouse held onto the wire was recorded. Ataxia and gait abnormalities were tested from the foot print pattern of the mouse.

Electroretinographic analysis

Full-field ERGs were recorded from homozygous *Pank2* and wild-type littermates as described previously (24,25). Briefly, for scotopic responses, mice were dark-adapted overnight and anesthetized with ketamine (87 mg/kg) plus xylazine (13 mg/kg). Pupils were dilated with 2.5% phenylephrine and 1% atropine in dim red-light and mice were kept on a warming blanket. Contact lens electrodes for mice were placed on the corneal surfaces bilaterally with 1% methylcellulose, and silver wire reference and ground electrodes were placed subcutaneously in the nose and tail, respectively. Using a UTAS-E 3000 Visual Diagnostic System (LKC Technologies, Gaithersburg, MD, USA) and beginning below ERG threshold, stimuli were presented in order of increasing luminance from −4.6 to +0.4 log cd s/m^2. In addition, scotopic a-waves were measured in response to a bright flash of +2.4 log cd s/m^2 at a 2-fold higher sampling rate to more accurately measure the amplitude. Three to 15 responses at each intensity were computer averaged. Interstimulus intervals ranged from 5 s at the lowest intensities to 120 s at the highest intensities. The amplitude of the a- and b-waves were measured.

Mice were then exposed to a background light of 30 cd m^{-2} for 10 min before recording photopic responses to stimuli presented at a rate of 2 Hz (for measurement of b-waves) and at

0.4 log cd s/m^2. Because photopic a-waves are negligible in mice (26), only the amplitude of the photopic b-waves was measured.

Pupil response measurement

Pupillary responses were measured from pigmented *Pank2* knock-out and wild-type littermate mice. Mice were dark-adapted for 90 min. Under dim red-illumination, unanesthetized mice were restrained in front of an infrared videocamera attached to a Hitachi Infrared CCD Camera using a rodent restraining device. A halogen microscope illuminator with a fiber optic bundle was used with a Kodak Wratten 47B filter placed in the light path to deliver a 470 nm stimulus to the contralateral eye and pupillary constriction was monitored under infrared light. The pupillary diameter was measured and used to calculate pupil area.

Immunohistochemistry

For immunostaining of the retina, enucleated eyes were fixed in 4% paraformaldehyde in PBS fixative for 2 h, transferred to 30% sucrose, flash frozen and sectioned (10 μm). Retinal and testis (described earlier) sections were immunostained with antibodies using standard procedures (27). Polyclonal anti-mouse Pank1A antibody was raised against a 14-mer peptide (PSELQPQPLFAQHD) in the first exon and was affinity purified with the peptide. Anti-OxPhos Complex V subunit β (Molecular Probes) was used as a mitochondrial marker. Testes paraffin sections were de-waxed, re-hydrated, steamed for 30 min in 1 m_M ethylenediaminetetraacetic acid followed by treatment with 5% hydrogen peroxide prior to staining. For adsorbed anti-Pank2, serum was pre-adsorbed with 10^{-5} $_M$ peptide, the same peptide against which the antibody was raised, for 48 h at 4°C. Staining was enhanced with ABC Elite Vector Stain Substrate Kit (Vector Laboratories) and visualized with 3,3′-diaminobenzidine (DAB substrate kit; Vector Laboratories). Sections were examined using a Nikon E800 microscope, and images were captured using a Spot II digital camera.

Statistical analysis

One-way ANOVA with Bonferroni's multiple comparison post-test was performed using Prism version 4.0a for Macintosh OS X (GraphPad Software, San Diego, CA, USA).

Acknowledgements

We are grateful to Matt LaVail, Donna Ferriero and Hannes Vogel for their insights and advice. We thank Juanito Meneses, Hernan Consengco, Doug Yasumura, Mike Matthes and Jose Velarde for excellent technical assistance and advice and members of our laboratories, particularly Monique Johnson, for helpful discussion and support. We thank Gerry Matson and Mark Knudsen, San Francisco Veterans Affairs Medical Center, CA for their MRI expertise. This work was funded by a grants from the NEI, Research to Prevent Blindness, and the Bernard A. Newcomb Macular Degeneration Foundation. J.G. is an investigator with the Howard Hughes Medical Institute.

References

1. Zhou B, Westaway SK, Levinson B, Johnson MA, Gitschier J, Hayflick SJ. A novel pantothenate kinase gene (*PANK2*) is defective in Hallervorden–Spatz syndrome. Nat Genet 2001;28:345–349. [PubMed: 11479594]
2. Dooling EC, Schoene WC, Richardson EP Jr. Hallervorden–Spatz syndrome. Arch Neurol 1974;30:70–83. [PubMed: 4808495]
3. Hortnagel K, Prokisch H, Meitinger T. An isoform of hPANK2, deficient in pantothenate kinase-associated neurodegeneration, localizes to mitochondria. Hum Mol Genet 2003;12:321–327. [PubMed: 12554685]
4. Johnson MA, Kuo YM, Westaway SK, Parker SM, Ching KHL, Gitschier J, Hayflick SJ. Mitochondrial localization of human PANK2 and hypotheses of secondary iron accumulation in pantothenate kinase-associated neurodegeneration. Ann N Y Acad Sci 2004;1012:282–298. [PubMed: 15105273]

5. Deng W, Lin H. *Miwi*, a murine homolog of *piwi*, encodes a cytoplasmic protein essential for spermatogenesis. Dev Cell 2002;2:819–830. [PubMed: 12062093]
6. Crawley, JN. What's Wrong with My Mouse?: Behavioral Phenotyping of Transgenic and Knockout Mice. Wiley–Liss; New York, NY: 2000. p. 31-45.p. 47-63.see also
7. Whiteley SJ, Young MJ, Litchfield TM, Coffey PJ, Lund RD. Changes in the pupillary light reflex of pigmented royal college of surgeons rats with age. Exp Eye Res 1998;66:719–730. [PubMed: 9657904]
8. Hayflick SJ, Westaway SK, Levinson B, Zhou B, Johnson MA, Ching KH, Gitschier J. Genetic, clinical, and radiographic delineation of Hallervorden–Spatz syndrome. N Engl J Med 2003;348:33–40. [PubMed: 12510040]
9. Afshar K, Gonczy P, DiNardo S, Wasserman SA. *Fumble* encodes a pantothenate kinase homolog required for proper mitosis and meiosis in *Drosophila melanogaster*. Genetics 2001;157:1267–1276. [PubMed: 11238410]
10. Castrillon DH, Gonczy P, Alexander S, Rawson R, Eberhart CG, Viswanathan S, DiNardo S, Wasserman SA. Toward a molecular genetic analysis of spermatogenesis in *Drosophila melanogaster*: characterization of male-sterile mutants generated by single P element mutagenesis. Genetics 1993;135:489–505. [PubMed: 8244010]
11. Nantel F, Monaco L, Foulkes NS, Masquilier D, LeMeur M, Henriksen K, Dierich A, Parvinen M, Sassone-Corsi P. Spermiogenesis deficiency and germ-cell apoptosis in CREM-mutant mice. Nature 1996;380:159–162. [PubMed: 8600390]
12. Blendy JA, Kaestner KH, Weinbauer GF, Nieschlag E, Schutz G. Severe impairment of spermatogenesis in mice lacking the CREM gene. Nature 1996;380:162–165. [PubMed: 8600391]
13. Bosl MR, Stein V, Hubner C, Zdebik AA, Jordt SE, Mukhopadhyay AK, Davidoff MS, Holstein AF, Jentsch TJ. Male germ cells and photoreceptors, both dependent on close cell–cell interactions, degenerate upon ClC-2 Cl (−)channel disruption. EMBO J 2001;20:1289–1299. [PubMed: 11250895]
14. Duncan JL, LaVail MM, Yasumura D, Matthes MT, Yang H, Trautmann N, Chappelow AV, Feng W, Earp HS, Matsushima GK, et al. An RCS-like retinal dystrophy phenotype in *mer* knockout mice. Invest Ophthalmol Vis Sci 2003;44:826–838. [PubMed: 12556419]
15. Lu Q, Gore M, Zhang Q, Camenisch T, Boast S, Casagrada R, Lai C, Skinner MK, Klein R, Matsushima GK, et al. Tyro-3 family receptors are essential regulators of mammalian spermatogenesis. Nature 1999;398:723–728. [PubMed: 10227296]
16. Shinohara T, Orwig KE, Avarbock MR, Brinster RL. Restoration of spermatogenesis in infertile mice by Sertoli cell transplantation. Biol Reprod 2003;68:1064–1071. [PubMed: 12604661]
17. Ripps H, Peachey NS, Xu X, Nozell SE, Smith SB, Liou GI. The rhodopsin cycle is preserved in IRBP 'knockout' mice despite abnormalities in retinal structure and function. Vis Neurosci 2000;17:97–105. [PubMed: 10750831]
18. Cole TB, Wenzel HJ, Kafer KE, Schwartzkroin PA, Palmiter RD. Elimination of zinc from synaptic vesicles in the intact mouse brain by disruption of the ZnT3 gene. Proc Natl Acad Sci USA 1999;96:1716–1721. [PubMed: 9990090]
19. Manabat C, Han BH, Wendland M, Derugin N, Fox CK, Choi J, Holtzman DM, Ferriero DM, Vexler ZS. Reperfusion differentially induces caspase-3 activation in ischemic core and penumbra after stroke in immature brain. Stroke 2003;34:207–213. [PubMed: 12511776]
20. Lu B, Bishop CE. Late onset of spermatogenesis and gain of fertility in POG-deficient mice indicate that POG is not necessary for the proliferation of spermatogonia. Biol Reprod 2003;69:161–168. [PubMed: 12606378]
21. Kuo YM, Gitschier J, Packman S. Developmental expression of the mouse mottled and toxic milk genes suggests distinct functions for the Menkes and Wilson disease copper transporters. Hum Mol Genet 1997;6:1043–1049. [PubMed: 9215673]
22. LaVail MM, Battelle BA. Influence of eye pigmentation and light deprivation on inherited retinal dystrophy in the rat. Exp Eye Res 1975;21:167–192. [PubMed: 1164921]
23. LaVail MM, Gorrin GM, Repaci MA, Thomas LA, Ginsberg HM. Genetic regulation of light damage to photoreceptors. Invest Ophthalmol Vis Sci 1987;28:1043–1048. [PubMed: 3596986]
24. Bok D, Yasumura D, Matthes MT, Ruiz A, Duncan JL, Chappelow AV, Zolutukhin S, Hauswirth W, LaVail MM. Effects of adeno-associated virus-vectored ciliary neurotrophic factor on retinal

structure and function in mice with a P216L rds/peripherin mutation. Exp Eye Res 2002;74:719–735. [PubMed: 12126945]

25. Vollrath D, Feng W, Duncan JL, Yasumura D, D'Cruz PM, Chappelow A, Matthes MT, Kay MA, LaVail MM. Correction of the retinal dystrophy phenotype of the RCS rat by viral gene transfer of Mertk. Proc Natl Acad Sci USA 2001;98:12584–12589. [PubMed: 11592982]
26. Peachey NS, Goto Y, al-Ubaidi MR, Naash MI. Properties of the mouse cone-mediated electroretinogram during light adaptation. Neurosci Lett 1993;162:9–11. [PubMed: 8121644]
27. Kuo YM, Su T, Chen H, Attieh Z, Syed BA, McKie AT, Anderson GJ, Gitschier J, Vulpe CD. Mislocalisation of hephaestin, a multicopper ferroxidase involved in basolateral intestinal iron transport, in the sex linked anaemia mouse. Gut 2004;53:201–206. [PubMed: 14724150]

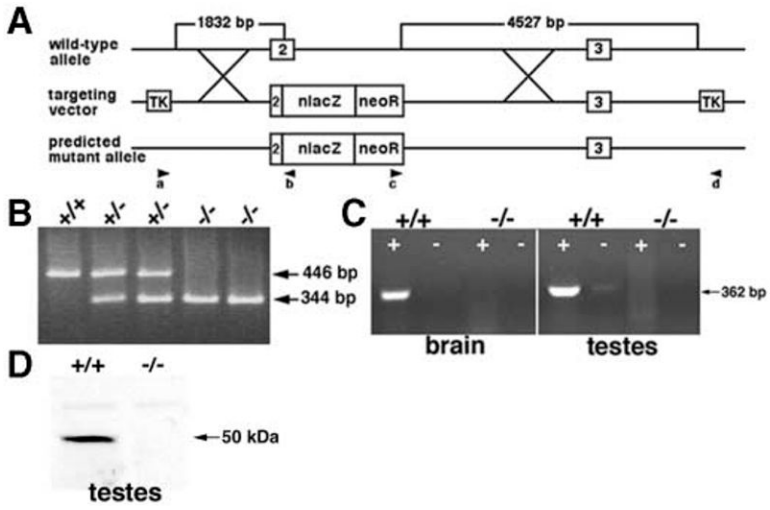

Figure 1.

Generation of *Pank2* knock-out animals. (**A**) Schematic illustration of the targeting strategy. Two portions of the murine *Pank2* gene (an 1832 bp fragment containing parts of intron 1 and exon 2 and a 4527 bp fragment spanning exon 3) were incorporated into the targeting vector. Homologous recombination in the regions indicated X resulted in the predicted mutant allele. Correctly targeted ES lines were assessed by PCR using pairs of primers (a+b and c + d). (**B**) Genotyping of F2 progeny by PCR using two pairs of primers, as described in Materials and Methods. The 446 bp fragment corresponds to the normal gene, and the 344 bp fragment is derived from the correctly targeted gene. Results from wild-type (+/+), heterozygous (+/−) and homozygous knock-out (−/−) mice are shown. (**C**) RT–PCR demonstrating the presence and absence of the expected 362 bp product from exons 2–4 of brain and testes RNA in wild-type (+/+) and *Pank2* (−/−) animals, respectively. White + and − symbols indicate with or without RT prior to PCR. (**D**) Western blot analysis of proteins from brain and testes extracts of wild-type (+/+) and mutant (−/−) animals with anti-Pank2 antibody. The predicted size for Pank2 is 50 kDa, and a band corresponding to this size is present in wild-type animals but absent in mutant animals.

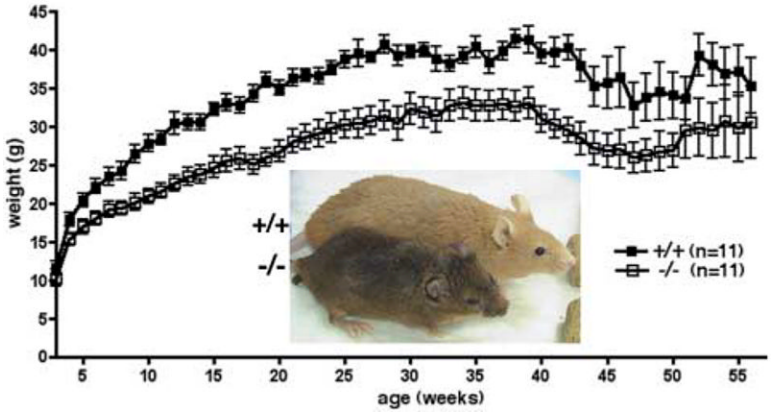

Figure 2.

Growth reduction in the *Pank2* null animals. Body weight (in grams) of the line 81 homozygous *Pank2* mice (open squares) is compared with that of the wild-type (solid squares) littermates as a function of age from weeks 3 to 56. Line graph shows mean ± SEM of body weight. Inset: Representative photograph of a wild-type and *Pank2* mouse at week 50. Weight and size differences in the 174 line were similar (data not shown).

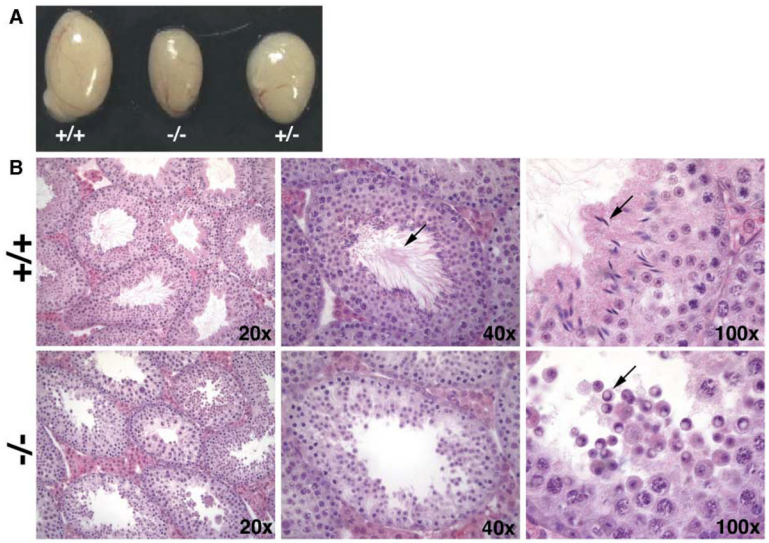

Figure 3.

Phenotypic analysis of wild-type and *Pank2* mutant testes. (**A**) Size comparison of representative testis from an 8-week-old wild-type (+/+) male with those from *Pank2* mutant (−/−) and heterozygote (+/−) littermates. Identical phenotypes were observed in both the 81 and 174 lines. (**B**) Histological analysis of testis sections from 8-week-old wild-type (+/+) and mutant (−/−) littermates stained with hematoxylin and eosin (H&E). Images were taken at 20×, 40× and 100× magnification. Arrows indicate mature spermatozoa (40×) and elongated spermatocytes (100×) in the wild-type animals and arrested, round, vaculated spermatids in the mutant. Although the testes of heterozygous mice were of intermediate size, the histochemical analysis of the testis was identical to wild-type.

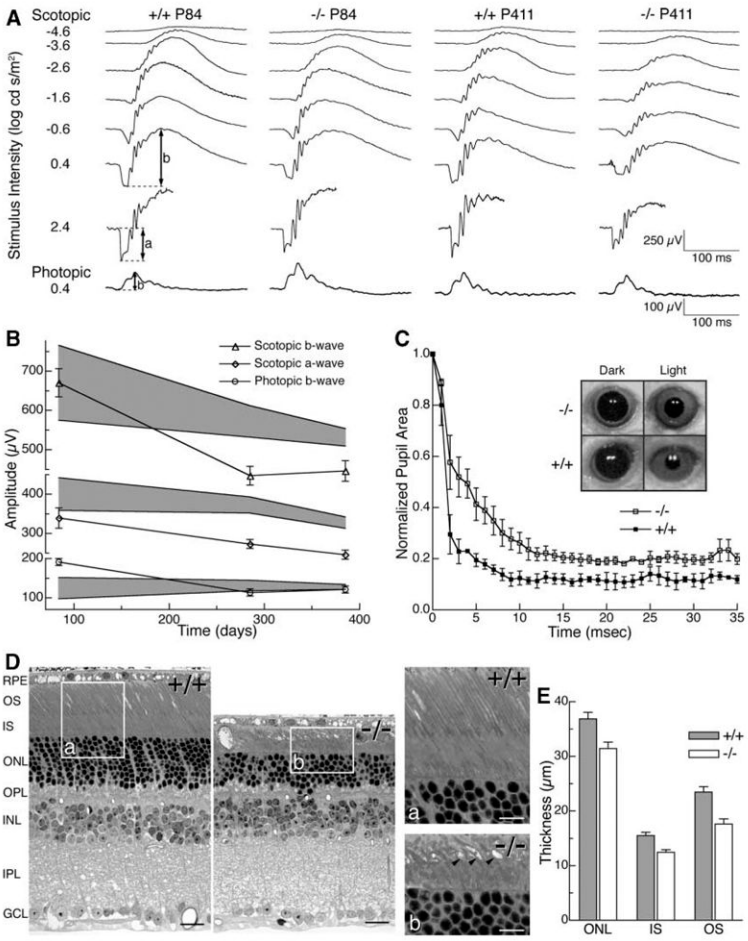

Figure 4.

Retinal abnormalities in the *Pank2* mutant. (**A**) Representative ERG waveforms recorded from wild-type (+/+) and *Pank2* (−/−) littermates at P84 and P411. The scotopic a- and b-wave amplitudes and photopic b-wave amplitude reported in (**B**) are indicated. Scotopic b-wave amplitudes and photopic b-wave amplitudes are measured in response to a standard flash of +0.4 log cd s/m^2, and scotopic a-wave amplitudes are measured in response to a bright flash of +2.4 log cd s/m^2 at a 2-fold higher sampling rate, resulting a shorter recorded duration. (B) Summary of ERG amplitude data for all animals tested. Shaded areas delineate wild-type (+/+) mean ± SEM amplitudes for scotopic b-waves (top zone), scotopic a-waves (middle zone) and photopic b-waves (bottom zone). Mean data for the mutant (−/−) are indicated by the open symbols ± SEM The numbers of wild-type and mutant eyes tested were six each at P84, six and 12, respectively, at P285, and 17 and 18, respectively, at P363–P430. Data for all animals of 1 year and older are collapsed into a single time point corresponding to the mean age of P385. (**C**) Pupillary responses were measured from *Pank2* (−/−, open symbol, $n = 4$) and wild-type (+/+, closed symbol, $n = 2$) littermate mice, age P285, after dark-adaptation for 90 min and exposed to a 470 nm stimulus. Pupillary area measurements were normalized to the average area measured over a 5 s pre-stimulus baseline and were recorded for 30 s after stimulus presentation. (C, Inset) Pictures showing reduced constriction in *Pank2* pupils before and after stimulus when compared with wild-type. (**D**) Light micrographs from albino wild-type and *Pank2* mice at P411. The *Pank2* retina shows disorganized and shorter outer segments (OS), shorter inner segments (IS) and a thinner outer nuclear layer (ONL) when compared with age-matched wild-type retina. Area of interest is expanded in insets a and b. Prominent vacuoles

are present in the *Pank2* OS, indicated by arrows in inset b. (**E**) Summary of retinal thickness data. Bar graphs show mean ± SEM of the thickness of ONL, IS and OS in wild-type (+/+, solid symbol, $n = 15$) and *Pank2* (−/−, open symbol, $n = 19$) animals aged P363–P430.

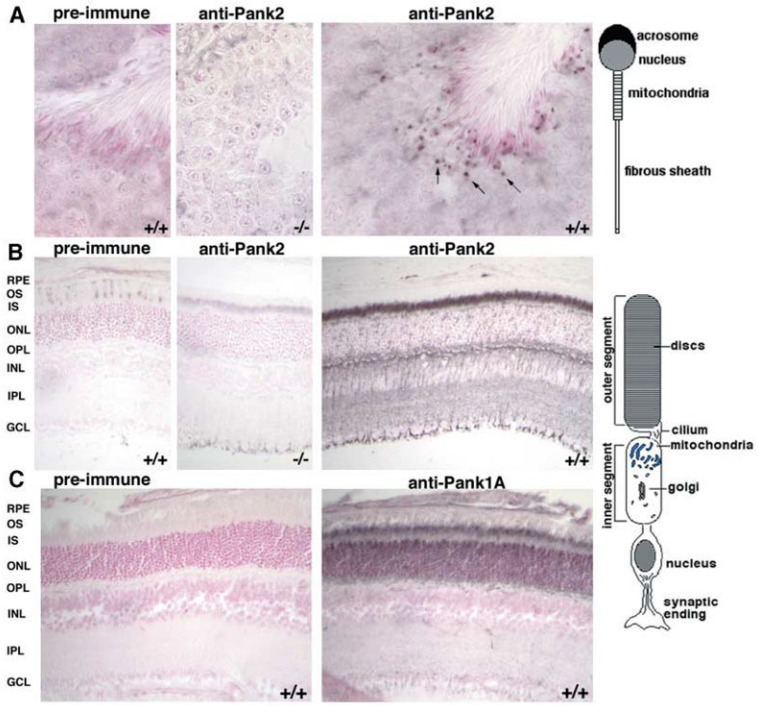

Figure 5.

Immunohistochemical localization of Pank2 in the testes and retina. (**A**) Localization of Pank2 in wild-type testes, demonstrating localization to spermatozoa (100×). The cartoon depicts the region of the spermatoza in which mitochondria are concentrated. (**B**) Localization of Pank2 in the retina (40×). Pank2 is highly expressed in the inner segment (IS) and also in the outer plexiform layer (OPL), inner nuclear layer (INL) and inner plexiform layer (IPL) (right). For reference, a drawing of the rod photoreceptor is presented. No staining is detected in the pre-immune control sera in either tissue (left panel) or in tissues from the mutant animals (middle panel). (**C**) Localization of Pank1A in the retina, demonstrating staining throughout the photoreceptor, unlike Pank2.